Transducer Placement for Broadband Active Vibration Control Using a Novel Multidimensional QR Factorization

Larry P. Heck
SRI International
Menlo Park, CA 94025

Koorosh Naghshineh
Western Michigan University
Kalamazoo, MI 49008

Julia A. Olkin
SRI International
Menlo Park, CA 94025

Abstract

This paper advances the state of the art in the selection of minimal configurations of sensors and actuators for active vibration control with smart structures. The method extends previous transducer selection work by (1) presenting a unified treatment of the selection and placement of large numbers of both sensors and actuators in a smart structure, (2) developing computationally efficient techniques to select the best sensor-actuator pairs for multiple *unknown* force disturbances exciting the structure, (3) selecting the best sensors and actuators over multiple frequencies , and (4) providing bounds on the performance of the transducer selection algorithms. The approach is based on a novel, multidimensional extension of the Householder QR factorization algorithm applied to the frequency response matrices that define the vibration control problem. The key features of the algorithm are its very low computational complexity, and a computable bound that can be used to predict whether the transducer selection algorithm will yield an optimal configuration *before* completing the search. Optimal configurations will result from the selection method when the bound is tight, which is the case for many practical vibration control problems. This paper presents the development of the method, as well as its application in active vibration control of a plate.

1 INTRODUCTION

Active vibration control represents the state of the art in reducing unwanted vibrations in structures. A current focus of research in the area is the development of smart materials that can automatically sense and then control vibrations induced from external disturbances. Smart materials for vibration control applications typically consist of embedded sensors, actuators, communication channels, and processors that have been programmed to implement the prescribed control law with the available transducers. However, current control algorithms cannot effectively deal with large system configurations (many sensors and actuators resulting in too many interconnections). Thus, subsets of transducers are often employed to achieve the desired control. Many of these presume the existence of a control configuration (i.e., layout of the sensors and actuators and the interconnections between them) or use ad-hoc methods to specify one, and focus instead on the design of the best control law. This is in spite of the fact that the complexity and performance of a control system are largely determined by the underlying control configuration (Nett and Spang, 1987).

Recent work in transducer selection algorithms can be broadly grouped into two approaches. The first approach assumes that permissible transducer locations are a continuous function in spatial location. Approaches to solve this problem utilize numerical optimization methods where the transducer locations are included as optimization parameters (Chen et al., 1991; Skelton and DeLorenzo, 1983; Wang et al., 1991). In general, these methods have high computational complexity, and, as a result, have been limited to small-scale transducer selection problems, focusing on either actuator or sensor selection (but not both). Specifically, the methods have been applied to problems of selecting tens of transducers at a single frequency.

The second transducer selection approach treats the problem where only a fixed (finite) number of transducer locations are permissible. Approaches to solve this discrete selection problem have focused on the use of heuristic search methods to treat the combinatorial explosion of candidate transducer configurations. Work in this area includes efforts by Snyder and Hansen (1990). In their paper, the authors focus on the sensor selection problem, and present an efficient least squares technique to evaluate the performance of each sensor configuration. However, the paper does not address the problem of efficiently searching through

all combinations and instead employs exhaustive search. As a result, the approach was limited to sensor selection only, at a single frequency. Ruckman and Fuller (1993) extended the work by Snyder and Hansen by focusing on selecting actuators (instead of sensors) and suggesting the use of the general body of subset selection methods. The subset selection methods include sequential search methods (e.g., forward and backward selection), which are computationally efficient but can yield unpredictably poor results. Finally, work by Baek and Elliott (1995) employed a class of heuristic search methods known as natural algorithms for the discrete transducer selection problem. The complexity of the search methods (simulated annealing and genetic algorithms) is much more efficient than exhaustive search, but significantly higher than the sequential search methods. While the methods provide a useful alternative to the sequential search methods (outperforming them in some cases), the computational complexity of the methods restrict their use to small-scale transducer selection problems.

This paper presents a new discrete transducer selection method for designing active vibration control configurations. First, the method extends previous transducer selection work by presenting a unified treatment of the selection and placement of large numbers of both sensors and actuators in a smart structure. Second, the new method has a very low computational complexity (lower than sequential forward selection) making it useful for very large-scale sensor and actuator selection problems (thousands of sensor-actuator pairs). Third, while all the approaches described above choose transducers assuming knowledge of the location of the excitation forces on the structure (and often limit the excitation to a point force), the method described in this paper does not require this knowledge. In this way, the best transducer locations can still be selected for applications where the locations of the disturbing forces are not known during the design of the transducer configuration. Fourth, the method presented here chooses the best actuators over multiple frequencies. Finally, the paper presents a computable bound that can be used to predict whether the transducer selection algorithm will yield an optimal configuration *before* completing the search. Optimal configurations will result from the selection method when the bound is tight, which is the case for many practical vibration control problems.

This paper is organized as follows. The next section briefly defines the vibration control problem and

specifies measures of performance that the control law uses. Section 3 formally defines the transducer selection problem in the context of this control law and proceeds to describe the new transducer selection approach. We also describe the complexity of the various selection methods, showing that the multidimensional QR algorithm is computationally more efficient than the other leading selection algorithms (including sequential forward selection). Finally, Section 4 presents results from application of this approach to a model of a smart plate (i.e., with embedded sensors and actuators).

2 VIBRATION CONTROL PROBLEM

In recent years, a variety of approaches have been developed for structural vibration control. A common requirement of these approaches is knowledge of transfer functions relating disturbances, sensors, and actuators to each other and to the areas on the structure that are to be controlled. Knowledge of the transfer functions can be achieved through measurements (i.e., on-line system identification), or through the use of structural models (e.g., finite element models). For a broad class of structures, the transfer functions can be described by a set of linear time invariant (LTI) differential equations. The *state-space* form is a popular compact representation that writes these equations in first-order form, i.e.,

$$\dot{\mathbf{x}} = J\mathbf{x} + K\mathbf{u} \tag{1}$$

$$\mathbf{y} = L\mathbf{x} + M\mathbf{u} \tag{2}$$

where J, K, L, and M are state matrix variables, u is a vector formed by stacking the N_d disturbances and N_a actuator control inputs, $\dot{\mathbf{x}}$ is an element state vector of first and second derivative terms, and $\mathbf{y}$ is a vector of N_s sensor outputs.

Taking the Fourier transform of the state-space system in Eq. (2) yields an equivalent representation in terms of the frequency response matrix or plant $H(\omega)$:

$$Y(\omega) = H(\omega)U(\omega) \ , \tag{3}$$

where

$$H(\omega) = L(j\omega I - J)^{-1}K \quad + M \ . \tag{4}$$

The frequency response matrix can be divided into four submatrices E, A, S, and C:

$$H(\omega) = \begin{bmatrix} E(\omega) & A(\omega) \\ S(\omega) & C(\omega) \end{bmatrix} \ , \tag{5}$$

where $E \in \mathcal{C}^{m \times n}$ is the complex disturbance transfer matrix that relates spatially distributed forces (or pressures) at the disturbance source to spatially distributed displacements (or velocities, accelerations) in the desired vibration control zone (structural locations where minimal vibrations are desired); $A \in \mathcal{C}^{m \times k}$ is the complex actuator transfer matrix relating control inputs (e.g., voltages) for all k candidate actuators to displacements in the desired control zone; $S \in \mathcal{C}^{l \times n}$ is the sensor transfer matrix relating spatially distributed forces at the disturbance source to l measured normal displacements at the candidate sensor locations on the vibrating structure; and $C \in \mathcal{C}^{l \times k}$ is the feedback coupling between the actuators and the sensors.

Figure 1 shows a block diagram of the vibration control problem. The responses from the disturbance to the sensors, S, are sent to the *compensator* W. The outputs, WS, are sent through the actuators, A, to the vibration control zone. In this particular control implementation, a feedforward neutralization filter, N, is used to "neutralize" the feedback coupling, C, between the actuators and sensors. This technique is called Q-parameterization, which has been used successfully in vibration control problems to simplify control design (Flamm et al., 1995). Thus, AWS is an estimate of the vibrations that reach the control regions directly, denoted by E. The problem, then, is to find a causal compensator, W, that minimizes the expression

$$\min_{W} \sum_{\omega=\omega_l}^{\omega_h} \| E - AWS \|_2^2 \quad \text{subject to} \sum_{\omega=\omega_l}^{\omega_h} \| WS \|_2^2 \ \leq \ c \ , \tag{6}$$

where ω_l and ω_h are the low and high cutoff frequencies of the control bandwidth, respectively, and c is a scalar specified by the designer. The constraints in this problem are to ensure that the controller is physically

realizable, i.e., that the energy in the actuator inputs, WS, does not saturate the actuators, and that the compensator is causal.

Methods currently exist to solve the control problem in Eq. (6). An efficient time-domain method for vibration and noise control problems that uses a *conjugate-gradient* minimization approach to find finite-impulse response (FIR) controllers is described by Flamm et al. (1995). The system, developed by Olkin et al. (1994) , has been used to design multiple-input/multiple-output controllers for broadband noise and vibration control with large spatial extent.

3 TRANSDUCER SELECTION

Referring again to Figure 1, the choice of the actuators will change the size and nature of the S and A frequency response matrices. Practical limitations on the number and placement of transducers often means that vibrations in the desired control zone and disturbance forces cannot be directly measured, nor can the forces be exactly reproduced. Satisfaction of the control objective will therefore depend on the ability of the transducers to estimate and then manipulate these vibrations at the desired control zones.

3.1 Mathematical formulation

For the transducer selection problem, the modified control objective using reduced numbers of actuators (Heck and Naghshineh, 1994) is given as

$$\min_{W,\Pi_a,\Pi_s} \sum_{\omega=\omega_l}^{\omega_h} \| E - A\,\Pi_a\,W\,\Pi_s\,S \|_2^2 \quad \text{subject to} \sum_{\omega=\omega_l}^{\omega_h} \| W\,\Pi_s\,S \|_2^2 \leq \quad c\,, \tag{7}$$

with the minimization completed over two additional parameters $\Pi_a \in I^{m\times N_a} \quad (N_a < m)$ and $\Pi_s \in I^{N_s\times n} \quad (N_s < n)$, where $I^{i\times j}$ is the set of all $i \times j$ binary-valued matrices. The parameters are called *actuator and sensor selectors*, respectively. The columns of Π_a and rows of Π_s are unit basis vectors corresponding to actuator and sensor locations (e.g., unit basis vector $\mathbf{u}_3 = [0\ 0\ 1\ 0\ 0]^T$ corresponds to the third

transducer position). An actuator selector matrix given as

$$\Pi_a = \begin{bmatrix} 1 & 0 \\ 0 & 0 \\ 0 & 1 \end{bmatrix} \tag{8}$$

would select the first and third actuator responses (columns) of A.

3.2 Key issues

The problem in Eq. (7) is difficult to solve directly because the quadratic cost function is non-differentiable. This arises because of the discontinuous nature of the selector matrices: either a transducer is selected, or it is not. As a result, the problem cannot be solved through direct extensions of the gradient-based optimization methods (such as the conjugate gradient method), and instead has been addressed through direct enumeration (search) methods. The complexity of the enumeration method is approximately the complexity of a complete controller design and performance assessment for one configuration multiplied by the number of possible transducer configurations. The number of possible configurations grows extremely rapidly as the complexity of the system increases.

For the transducer selection problem, given m candidate sensors and n candidate actuators, the number of distinct subsystems with k sensors and l actuators will be

$$\binom{m}{k}\binom{n}{l} \triangleq \frac{m!}{k!(m-k)!}\frac{n!}{l!(n-l)!} . \tag{9}$$

The total number of distinct subsystems will be

$$\sum_{k=1}^{m}\sum_{l=1}^{n}\binom{m}{k}\binom{n}{l} , \tag{10}$$

where each subsystem corresponds to a selected subset of the candidate transducers.

Even for modest-size problems, the number of candidate transducer configurations in Eq. (10) becomes exceedingly large. For example, the number of possible configurations or subsystems in a system with 40 sensors and 40 actuators is approximately 1.1e+23 (assuming only subsystems with equal numbers of sensors and actuators are considered). To put this into perspective, if each configuration could be evaluated in 1 second (i.e., a complete control design with the compensator computed), then it would take over 3.4e+13 centuries to evaluate every possible configuration! As a result of the large numbers of possible transducer configurations, a practical method for transducer selection will necessarily consist of suboptimal, but highly efficient measures to assess controller quality along with fast enumeration algorithms.

3.3 Transducer selection approach: single frequency

The approach to transducer selection presented in this section employs computationally efficient heuristic methods that avoid the high combinatorics described above. The approach consists of two main steps. First, the problem shown in Eq. (7) is broken down into smaller, more tractable problems. Then, after the large set of candidate transducer configurations is reduced to a small number, full controller designs are completed. In the first step, the approach seeks submatrices of A and S selected by Π_a and Π_s that *extract the non-redundant* components of the original matrices. In addition, it is assumed that the residual error of the controller with these full matrices can be made small, i.e., $E \approx AWS$ at all frequencies. Beginning with the single frequency case, the approach approximates the controller with selected transducers such that $A\Pi_a W \Pi_s S \approx AWS$. To achieve this, a subspace distance measure, D_s, can be employed to quantify the difference between the original and candidate submatrices. A popular measure in the statistics, numerical analysis, and signal processing literature (Golub and Van Loan, 1989) is given as

$$D_s(A, A\Pi_a) = \sin\Theta(\mathcal{R}(A), \mathcal{R}(A\Pi_a)) \tag{11}$$

$$D_s(S, \Pi_s S) = \sin\Theta(\mathcal{R}(S^T), \mathcal{R}((\Pi_s S)^T)) \ , \tag{12}$$

where $\mathcal{R}$ denotes range space, and $\sin\Theta$ is the sine of the largest *principal angle* between the range subspaces of the transfer function matrices. The largest principal angle between two subspaces F and G is the angle between the unit vector in F whose orthogonal projection onto G gives the largest residual. The sine of the largest principal angle is equivalent to the 2-norm of the difference (residual) between the orthogonal projections onto the range spaces of the matrices.

Since the largest principal angle corresponds to a worst-case residual, it can be argued that the selector matrices should be chosen to make the distance measures in Eqs. (11) and (12) as small as possible. However, for the vibration control problem, such an approach could lead to large actuator inputs, which would violate the constraints in Eq. (7). To see this, consider the following example (Golub and Van Loan, 1989). Let $S, \Pi_s = I$ in Eq. (7), where I is the identity matrix. Also, let $\omega = \omega_q$ so that the minimization is completed over a single frequency. We can rewrite the minimization problem as

$$\min_{W,\Pi_a} \| E - A\,\Pi_a\,W \|_2^2 \quad \text{subject to} \| W \|_2^2 \leq c\,. \tag{13}$$

If the goal is to find the two best actuators, and

$$A = \begin{bmatrix} 1 & 1 & 0 \\ 1 & 1+\epsilon & 1 \\ 0 & 0 & 1 \end{bmatrix}, \quad E = \begin{bmatrix} 1 \\ -1 \\ 0 \end{bmatrix}, \tag{14}$$

then choosing the first two actuators (first two columns of A) gives the residual $\| E - A\Pi_a \|_2^2 = 0$, but $\| (A\Pi_a)^\dagger E \|_2^2 = \| \mathbf{W}_{LS} \|_2^2 = \mathcal{O}(1/\epsilon)$, where $Q^\dagger$ is the Moore-Penrose pseudoinverse operator (Stewart, 1984). As ϵ gets smaller, the actuator weights will grow and eventually violate the constraint in Eq. (13). On the other hand, the other two possible subsets of actuators will lead to small weight norms, but with a much worse residual.

This example highlights the tradeoff that exists between choosing an independent set of actuators and choosing a set that minimizes the residual control error. A similar tradeoff occurs in the use of *subset selection*

methods (Golub et al., 1976) to solve general rank-deficient least-squares problems. A solution developed for this problem uses a Householder QR with column-pivoting factorization. For the transducer selection problem, the factorization can be used to efficiently find an independent set of actuators and sensors. In addition, if the proper number of transducers is selected, the residuals in Eq. (7) can be made small.

The Householder QR algorithm can be described as follows. Let $G \in \mathcal{C}^{m \times n}$ matrix be representative of the A and S matrices in Eqs. (11) and (12). The QR decomposition of G can be written as

$$\begin{aligned} G &= QR \\ &= Q \begin{pmatrix} R_{11} & R_{12} \\ 0 & R_{22} \end{pmatrix} , \end{aligned}$$

where $Q \in \Re^{m \times m}$ has orthonormal columns ($Q^T Q = I$), R_{11} is a $k \times k$ matrix with a condition number approximately equal to σ_1/σ_k, $\| R_{22} \|$ is of the order σ_{k+1}, and k is the rank of G. Pivoting (or permuting) the columns of the QR factorization can be used to make R_{22} small. For a rank-deficient matrix with $r = \text{rank}(G)$, column pivoting can yield

$$Q^T G P = \begin{bmatrix} R_{11} & R_{12} \\ 0 & 0 \end{bmatrix} , \tag{15}$$

where $R_{11} \in C^{r \times r}$ is upper triangular and nonsingular, and $R_{12} \in C^{n-r \times r}$. With the column partitionings $GP = [g_{p_1}, g_{p_2}, \ldots, g_{p_n}]$ and $Q = [q_1, q_2, \ldots, q_m]$, and r_{ij} denoting the (i,j)-th element of R, we have

$$g_{p_k} = \sum_{i=1}^{min\{r,k\}} r_{ik} q_i \in \text{span}\{q_1, q_2, \ldots, q_r\} \quad \text{for } k = 1 : n . \tag{16}$$

This implies that the range(G) = span$\{q_1, \ldots, q_r\}$ = span$\{g_{p_1}, \ldots, g_{p_r}\}$. In other words, column pivoting can be used to find a subset of columns in a rank-deficient matrix that has the same range space as the original matrix, making the principal angles between the original and submatrix go to zero. In addition, the Householder procedure described in Golub and Van Loan (1989) ensures that the resulting submatrix of G is

also well-conditioned (i.e., that the columns are sufficiently independent). Selecting actuators, for example, with this procedure (columns of A in Eq. (7)) will make the distance measure in Eq. (11) go to zero and yield a subset with the same *control authority* as the original, densely packed set of actuators.

In most vibration control problems of interest, the rank of the A and S^T matrices will not be exactly zero. Rather, because of numerical approximations, the rank can only be specified in terms of a threshold on singular values, called the *numerical rank* (Stewart, 1984). A consequence is that nonzero differences will exist between the range spaces of the original and selected submatrices. As a result, a method is required to determine the circumstances under which the differences between the range spaces is small. A useful bound (Golub and Van Loan, 1989) can be determined that specifies these circumstances, i.e.,

$$\sin\Theta(A, A\Pi_a) \leq \sigma_{r+1} \parallel R_{11}^{-1} \parallel \tag{17}$$

$$\sin\Theta(S^T, (S\Pi_s)^T) \leq \sigma_{s+1} \parallel R_{11}^{-1} \parallel \ , \tag{18}$$

where σ_{r+1} and σ_{s+1} are the $(r+1)$st and $(s+1)$st largest singular values of A and S, respectively, and the submatrix R_{11} (this in general will be a different matrix for A and S) in the QR factorizations is guaranteed to be of the order σ_r^{-1} for A and σ_s^{-1} for S. These bounds show a sufficient condition for small errors; i.e., if there exists a large gap in successive singular values, called the *spectral gap*, then the error will be small. For transducer selection, these bounds provide a useful criterion for the optimality of a given configuration. Also, they give a direct correspondence between the numerical rank of the frequency response matrices and the number of required transducers; e.g., if the numerical rank of the actuator frequency response matrix is k, then k actuators are required.

3.4 Broadband extension

The goal for the broadband transducer selection problem is to minimize the expression in Eq. (7) with a single configuration over all frequencies of interest. For the broadband case, we extend the Householder procedure to compute factorizations over multiple matrices. The approach is as follows. Assume for some k

and frequency ω_i that we have computed Householder matrices $H_1, \ldots, H_{k-1}$ and permutations $P_1, \ldots, P_{k-1}$ such that

$$(H_{k-1}(\omega_i) \cdots H_1(\omega_i))G(\omega_i)(P_1(\omega_i) \cdots P_{k-1}(\omega_i)) = R^{k-1}(\omega_i) \tag{19}$$

$$= \begin{bmatrix} R_{11}^{(k-1)}(\omega_i) & R_{12}^{(k-1)}(\omega_i) \\ 0 & R_{22}^{(k-1)}(\omega_i) \end{bmatrix}, \tag{20}$$

where $R_{11}^{(k-1)}(\omega_i) \in C^{(k-1)\times(k-1)}$, $R_{12}^{(k-1)}(\omega_i) \in C^{(n-k+1)\times(k-1)}$, and $R_{22}^{(k-1)}(\omega_i) \in C^{(n-k+1)\times(m-k+1)}$. The single-frequency Householder method moves the column of G corresponding to the largest column in $R_{22}(\omega_i)$ to the kth column position (the lead position in the $R_{22}(\omega_i)$ matrix), where largest is specified by the selection of a vector norm. The column exchanges are accomplished with the permutation matrix $P(\omega_i)$. This is followed by a left multiplication by a Householder matrix that zeroes all the subdiagonal components of the largest $R_{22}(\omega_i)$ column vector. The procedure stops when $k - 1 = \text{rank}(G(\omega_i))$.

For the broadband case (multiple G matrices), instead of permuting a $G(\omega_i)$ based on the column with the largest vector norm in $R_{22}^{(k-1)}$, we permute $G(\omega_1), \ldots, G(\omega_n)$ based on one of eight possible performance measures on the matrix consisting of a column from each $R_{22}(\omega_1), \ldots, R_{22}(\omega_n)$ matrix.

These performance measures, discussed and analyzed in more detail in Olkin, Heck, and Naghshineh (1996) , can be selected depending on the application. The first four performance measures are the three induced matrix norms, l_1, l_2 and l_∞ and the Frobenius norm. The fifth performance measure chooses the smallest singular value of each actuator which helps minimize the effect of deep nulls in an actuator frequency response, which can lead to nonrobust control designs with poor performance. The sixth measure chooses the actuator response with the largest average value over all frequencies and response locations. The seventh measure is the ratio of the minimum to maximum actuator response over frequency, reflecting the fact that flatter actuator frequency responses are often desirable due to noise control robustness and performance considerations. The last performance measure attempts to minimize the effect of spatial nulls by choosing the maximum row sum of the actuator matrix.

As was the case with a single matrix, this permutation step is followed by left multiplying each $G(\omega_1)$, ..., $G(\omega_n)$ with the corresponding Householder matrices that will zero the subdiagonal components of the selected columns for each $R_{22}(\omega_1), \ldots, R_{22}(\omega_n)$ matrix. Figure 2 illustrates this multidimensional broadband extension of the Householder QR factorization with column pivoting. Note that P is not a function of frequency; hence this matrix of ones and zeros is the same for each frequency.

For the broadband case, the error bounds in Eqs. (17) and (18) hold for each frequency, i.e.,

$$\begin{aligned}
\sin\Theta(A(\omega_1), A(\omega_1)\Pi_a) &\leq \sigma_{r+1}(\omega_1) \parallel R_{11}(\omega_1)^{-1} \parallel \\
\sin\Theta(A(\omega_2), A(\omega_2)\Pi_a) &\leq \sigma_{r+1}(\omega_2) \parallel R_{11}(\omega_2)^{-1} \parallel \\
&\vdots \\
\sin\Theta(A(\omega_n), A(\omega_n)\Pi_a) &\leq \sigma_{r+1}(\omega_n) \parallel R_{11}(\omega_n)^{-1} \parallel
\end{aligned}$$

and

$$\begin{aligned}
\sin\Theta(S(\omega_1)^T, (S(\omega_1)\Pi_s)^T) &\leq \sigma_{s+1}(\omega_1) \parallel R_{11}(\omega_1)^{-1} \parallel \\
\sin\Theta(S(\omega_2)^T, (S(\omega_2)\Pi_s)^T) &\leq \sigma_{s+1}(\omega_2) \parallel R_{11}(\omega_2)^{-1} \parallel \\
&\vdots \\
\sin\Theta(S(\omega_n)^T, (S(\omega_n)\Pi_s)^T) &\leq \sigma_{s+1}(\omega_n) \parallel R_{11}(\omega_n)^{-1} \parallel \ .
\end{aligned}$$

The bounds hold for each frequency because the derivation of the bounds does not depend upon the specific properties of the QR factorization. Rather, the proof holds for a general R_{11} matrix. However, the quality of the bound may be adversely affected if $\parallel R_{11}^{-1} \parallel$ is not on the order of σ_k^{-1}.

3.5 Computational complexity of approach

The algorithm for implementing the transducer selection approach described above is computationally efficient and, as a result, can be used for very large-scale problems involving hundreds to thousands of sensors and

actuators. Specifically, suppose we are choosing k actuators out of N_d total actuators, with N_e error sensors, over N_f frequencies. Each of the following transducer selection methods requires some sort of computation of the residual of the active vibration control system. Let $\mathcal{O}(\text{residual})_k$ represent the flop count for computing the system residual with k actuators. Then Table 1 gives a general complexity overview of some actuator selection methods, and the dominating term by way of easy comparison. The methods are (i) Exhaustive Search, in which all combinations of k actuators are considered, (ii) Best k, in which each actuator is evaluated individually and the Best k are chosen, (iii) sequential forward selection, in which actuators are added to the chosen set based on which new actuator will behave the best with those already chosen, and finally, (iv) Multidimensional QR, the algorithm presented in this paper. Choosing k out of N_s sensors yields similar relative complexity counts as in Table 1, with Multidimensional QR still more computational efficient than the SFS method. For brevity, we include results for the actuators only.

Table 1: Algorithm Complexity For Choosing k out of N_d Actuators

Method	**General Complexity**	**Dominating Term**
Exhaustive Search	$N_f \frac{N_d!}{k!(N_d-k)!}\mathcal{O}(\text{residual})_k$	$N_f \frac{N_d!}{k!(N_d-k)!}(6N_e k^2 + 20k^3)$
Multidim. QR	$\sum_{i=1}^{k} i\mathcal{O}(\text{column-selection}) +$ $N_f\mathcal{O}(\text{Householder transform})$	$k^2(N_f N_e^2 + N_e^3) + kN_f N_e^3 + N_f N_e$
Seq. Forward Sel.	$\sum_{i=1}^{k}\{(N_d - i + 1)\mathcal{O}(\text{residual})_i\}$	$k^3 N_f N_d N_e + k^4 N_f N_d - k^5 N_f$
Best k	$N_d N_f \mathcal{O}(\text{residual})_1$	$7N_f N_d N_e$

It can be difficult to compare the dominating terms, so as way of example, consider a system with 40 possible actuators in which only 20 can be kept. Assume there are 20 error sensors measuring the actuator responses over 300 frequencies. Then the complexity for these four methods are shown in Table 2, printed in order of optimality of solution.

Table 2: Example Complexity Comparison

Method	**Complexity**
Exhaustive Search	6.9e19
Sequential Forward Selection	3.8e9
Multidimensional QR	9.9e7
Best k	1.7e6

Notice that the Multidimensional QR algorithm is more efficient than sequential forward selection, and comparable with Best K. In addition, the method is guaranteed to perform as well or better than both SFS and Best K. As will be demonstrated in the next section, the efficiency of this procedure enables practical transducer selection for large-scale problems.

4 NUMERICAL RESULTS

The methods described in the previous section were applied to the problem of controlling vibrations on a smart plate model (embedded sensors and actuators). The SPICES consortium's solid-plate model (Flamm et al. 1995) was considered.

As shown in Figure 3, the plate is a layered composite material $46 \times 46 \times 1.2$ cm. ($18 \times 18 \times 0.5$ in.), connected to an infinite, rigid base on the bottom of the plate at the four corners (indicated by the black dots). The plate was excited with a point force with x, y, and z components. The force was applied to the plate through a stiff tripod (all three connections with the plate move together to simulate connectors between the plate and attached machinery). The forcing function was an impulse with flat frequency response. The first 268 natural frequencies and mode shapes of this 3858-node plate model were used in the computation of frequency response matrices (admittance) relating excitation force to displacement.

The sensor models used in this numerical experiment measure point displacements. For the sensor placement studies, 361 evenly spaced candidate sensor locations were used. The candidate locations were on a 19×19 grid (2.5 cm=1 in. from nearest neighbor) in the middle layer (denoted by the dashed line). For the actuator placement studies, simple two-dimensional actuators were modeled and incorporated into the plate model. The actuators have length and depth (into the plate), but no width. Figure 4 shows a cross-section side view of the plate with an embedded actuator. The directional forces in the model are shown as $\pm F$, which produce an effective bending moment about the center of the actuator. A total of 180 candidate actuator locations were specified for the actuator selection studies. From a top view of the plate (xy projection), the actuator locations formed a checkerboard pattern, as illustrated in the right plot in Figure 3. The lines

between the dots on the checkerboard pattern represent the actuators, and all horizontal and vertical lines, represented by letters in this schematic, are considered actuators. The goal of the vibration control system was to reduce the transmission of forces over 500-4000 Hz from the tripod excitation to the connectors at the four corners of the plate. Thus, the four corners of the plate model represent the vibration control zone. All control law designs used FIR implementations designed using the conjugate-gradient method described in Section 2. The FIR weights were found by solving the minimization problem in Eq. (6).

To select the sensors and actuators, the continuous, time-domain, state-space model responses were sampled and used to compute the frequency response matrices S and A in Eq. (7). The sensor and actuator selction was then performed using these matrices. Finally, the FIR controller was implemented and the controlled system responses computed.

The S matrix consisted of 361 rows (corresponding to sensor responses), and the A matrix had 180 columns (actuator responses). The broadband extension of the Householder QR with column-pivoting factorization was applied to these matrices to find the columns of A and rows of S that formed matrices with approximately the same range space as the original matrices. As described in Section 3.4, the matrix 2-norm was used by the Householder algorithm to select the columns of the response matrices. The numerical rank of the S matrix (with a threshold set @ -30 dB) was approximately 3. Based on this, three sensors were chosen. Their locations correspond to the connector points between the tripod and the plate in Figure 3. The numerical rank of the A matrix was approximately 4. The left plot in Figure 5 shows the locations of the actuators and sensors chosen by the broadband QR method. The right plot shows the uncontrolled (dashed) and controlled (solid) time-domain impulse responses for the control bandwidth at the $x = 17$ in., $y = 17$ in. connector. As can be seen, this control configuration quickly reduces the vibration transmission from the tripod to the connectors. Figure 6 shows the power spectral density (psd) of the uncontrolled and controlled vibration responses for the sensor-actuator layout chosen by the multidimensional QR algorithm. The lines shown represent the root mean squared (RMS) of the values of the responses at all four feet from the x, y, and z tripod excitation. As can be seen, the controller effectively reduces the transmission power over the control bandwidth (500-4000 Hz).

To compare the QR-based designs with manually selected actuator locations, additional designs were completed, chosen to be intuitively competitive. The results are shown in Figures 7 through 10 (all cases used the QR sensor configuration). As can be seen, the performance for each design were inferior to those of the QR-based actuator configuration. Table 3 shows the in-band control performance (500-4000Hz) at each of the four feet (or corners) of the plate in dB. The three configurations of actuator placement are the QR-based configuration and the two comparison configurations shown in Figures 7 and 9. Notice that the performance at all four corners for the QR-based configuration is about the same level, whereas there is much more variation for the other two configurations, and even some enhancement.

Table 3: Performance Comparison.

	In-Band Performance (dB)			
Configuration	**Corner 1**	**Corner 2**	**Corner 3**	**Corner 4**
QR	10.9	10.9	11.4	11.4
Figure 7	6.86	-.24	.76	-.40
Figure 9	10.6	5.8	2.3	3.2

5 SUMMARY

This paper has presented a computationally efficient, unifying method for broadband sensor and actuator selection. The method is based on the Householder QR with column-pivoting factorization of the system's frequency response matrices. Using the Householder algorithm, upper bounds were presented on the errors induced by selecting a subset of transducers. The bounds can be computed efficiently, as they are in terms of the singular values of the response matrices. Also, they serve as sufficient conditions for optimality of the transducer selection method, such that rank-deficient response matrices with large spectral gaps in the singular values cause the bounds in Eq. (17) and Eq. (18) to reach equality instead of inequality. Finally, the multidimensional extension of the Householder QR procedure developed in this paper provides a practical method of selecting sensors and actuators that yield effective control over a broad band of frequencies. The new method is more efficient than sequential forward selection and has an order of complexity approaching

that of simply choosing the best K transducers independently. However, the new method performs as well or better than both competing algorithms. Future work will extend this method to minimize the required interconnections between the sensors and actuators.

6 ACKNOWLEDGEMENTS

This work was supported by ARPA Contracts MDA972-93-2-0010 and N00014-94-C-0176. The authors wish to thank the SPICES team for providing the plate model used in the numerical experiments presented here, and David Flamm, Bill Nowlin, Paul Titterton, and Ken Chou for helpful discussion related to this work.

7 REFERENCES

K. Baek, S. Elliott, 1995, "Natural algorithms for choosing source locations in active control systems," *ASME J. Sound and Vib.*, vol. 186, no. 2, pp. 245–267.

G. Chen, R. Bruno, and M. Salama, 1991, "Optimal placement of active/passive members in truss structures using simulated annealing," *AIAA Journal*, vol. 29, no. 8.

R. Clark and C. Fuller, 1992, "Optimal placement of piezoelectric actuators and polyvinylidence fluoride error sensors in active structural acoustic control approaches," *J. Acoust. Soc. Am.*, vol. 92(3), pp. 1521–1533.

D. Flamm, L. Heck, P. Titterton, W. Nowlin, J. Olkin, and K. Chou, 1995, "Control system design for the spices smart structure demonstrations," in *SPIE Conference on Smart Structures and Materials*, pp. 237–248.

G. H. Golub, V. Klema, and G. W. Stewart, 1976, "Rank degeneracy and least squares problems," Tech. Rep. TR-456, Depart. of Computer Science, University of Maryland, College Park, MD.

G. H. Golub and C. F. Van Loan, 1989, *Matrix Computations*. Baltimore: The Johns Hopkins University Press, second ed.

L. Heck and K. Naghshineh, 1994, "Large-scale, broadband actuator selection for active noise control," in *Proceedings of Nat. Conf. in Noise Control Engineering*, (Ft. Lauderdale, FL).

C. Nett and H. Spang, 1987, "Control structure design: A missing link in the evolution of modern control theories," in *American Control Conference*, vol. 29.

J. A. Olkin, M. S. Freed, and P. D. Jungers, 1994, "SRI weights algorithm and performance simulation (SWAPS) code.," tech. rep., SRI International.

J. Olkin, L. Heck, and K. Naghshineh, 1996, "Automated placement of transducers for active noise control: Performance measures," in *International Conference on Acoustics, Speech, and Signal Processing*, (Atlanta, GA). C. Ruckman and C. Fuller, 1993 "Optimizing actuator locations in feedforward active control systems using subset selection," in *Supplement to 2nd Conf. on Recent Advances in Active Control of Sound and Vibration*, pp. S122–S133.

K. Skelton, R.E. DeLorenzo, M.L., 1983, "Selection of noisy actuators and sensors in linear stochastic systems," *Journal of Large Scale Systems, Theory, and Applications*, vol. 4, pp. 109–136.

S. D. Snyder and C. H. Hansen, 1990, "Using multiple regression to optimize active noise control system design," in *J. of Sound and Vib.*.

G. W. Stewart, 1984, "Rank degeneracy," *SIAM J. Sci. Statist. Comput.*, vol. 5, pp. 403–413.

B. Wang, R. Burdisso, and C. Fuller, 1991, "Optimal placement of piezoelectric actuators for active control of sound radiation from elastic plates," *Proceedings of Nat. Conf. in Noise Control Engineering*, pp. 267–274.

B. Wang, 1996, "Optimal placement of microphones and piezoelectric transducer actuators for far-field sound radiation control," *J. Acoust. Soc. Am.*, vol. 99, no. 5.

Table Legends

Table 1: Algorithm Complexity For Choosing k out of N_d Actuators.

Table 2: Example Complexity Comparison.

Table 3: Performance Comparison.

Figure Legends

Figure 1: Block diagram of the vibration control problem. The responses from the disturbance to the sensors, S, are sent to the *compensator* W. The outputs, WS, are sent through the actuators, A, to the vibration control zone. A feedforward neutralization filter, N, is used to "neutralize" the feedback coupling, C, between the actuators and sensors.

Figure 2: Multidimensional Householder QR factorization with column pivoting.

Figure 3: The left plot shows the solid-plate model developed by the SPICES consortium. The right plot shows the pattern for the 180 candidate actuator locations embedded in the SPICES plate.

Figure 4: Actuator Model.

Figure 5: Locations of the actuators and sensors chosen by the broadband QR method (left). The uncontrolled (dashed) and the controlled (solid) time-domain impulse responses for the control bandwidth for the connector located at $x = 17in.$, $y = 17in.$ (right).

Figure 6: Plot of the RMS values of the uncontrolled (solid) and the controlled (dashed) responses at all four feet for the configuration chosen by the QR algorithm.

Figure 7: Locations of the actuators and sensors chosen by the authors for comparison to the QR method (left). The uncontrolled (dashed) and the controlled (solid) time-domain impulse responses for the control bandwidth for the connector located at $x = 17in.$, $y = 17in.$ (right).

Figure 8: Plot of the RMS of the uncontrolled (solid) and the controlled (dashed) responses at all four feet for the configuration chosen by the authors.

Figure 9: Locations of the actuators and sensors chosen by the authors for comparison to the QR method (left). The uncontrolled (dashed) and the controlled (solid) time-domain impulse responses for the control bandwidth for the connector located at $x = 17in.$, $y = 17in.$ (right).

Figure 10: Plot of the RMS of the uncontrolled (solid) and the controlled (dashed) responses at all four feet for the configuration chosen by the authors.

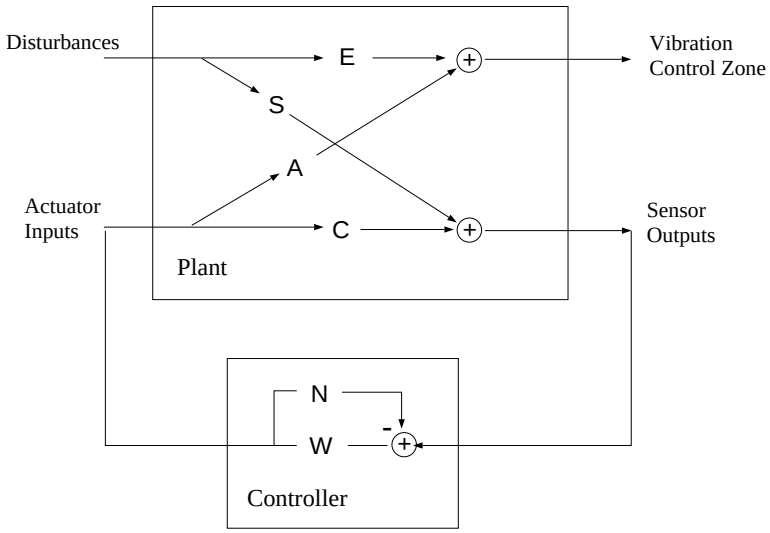

Figure 1: *Block diagram of the vibration control problem. The responses from the disturbance to the sensors, S, are sent to the compensator W. The outputs, WS, are sent through the actuators, A, to the vibration control zone. A feedforward neutralization filter, N, is used to "neutralize" the feedback coupling, C, between the actuators and sensors.*

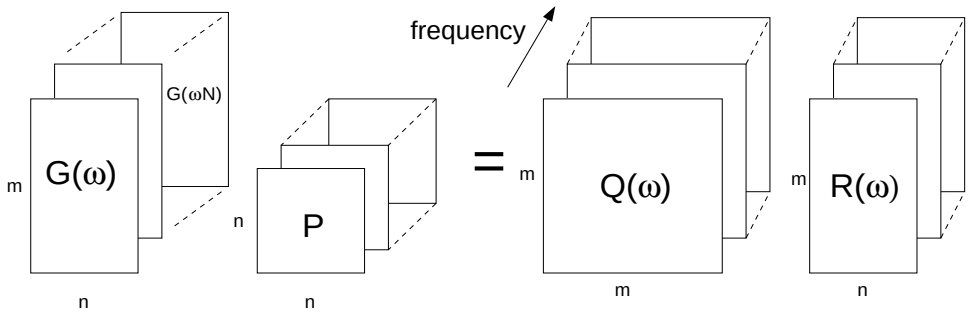

Figure 2: *Multidimensional Householder QR factorization with column pivoting.*

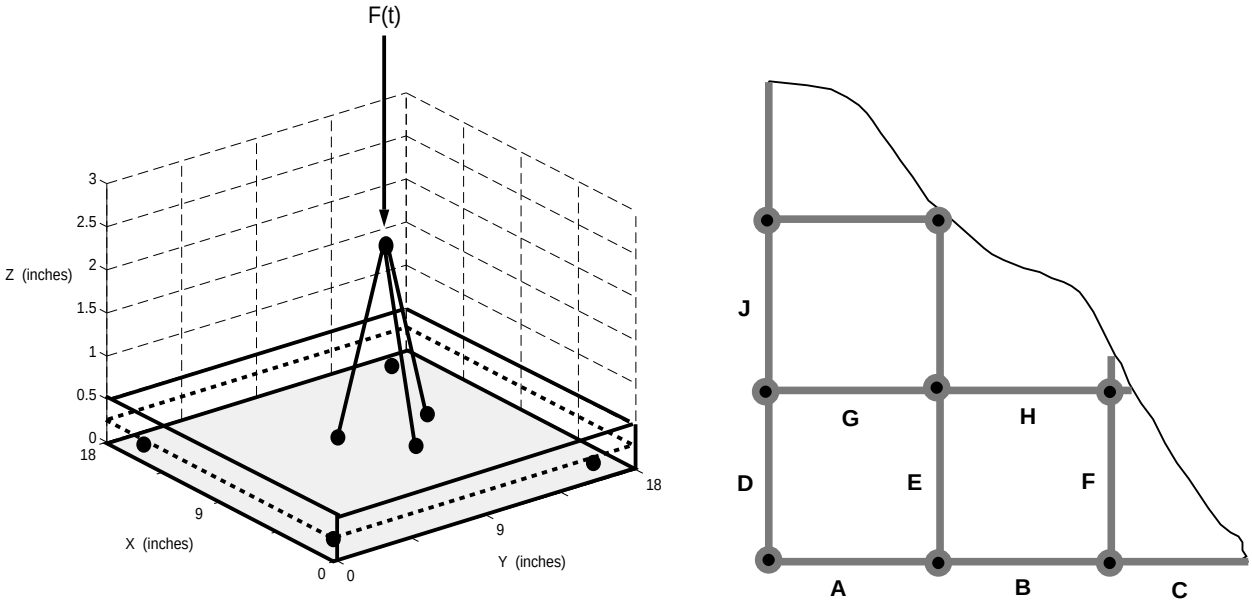

Figure 3: *The left plot shows the solid-plate model developed by the SPICES consortium. The right plot shows the pattern for the 180 candidate actuator locations embedded in the SPICES plate.*

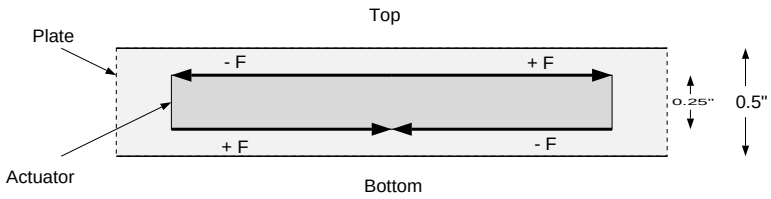

Figure 4: *Actuator Model.*

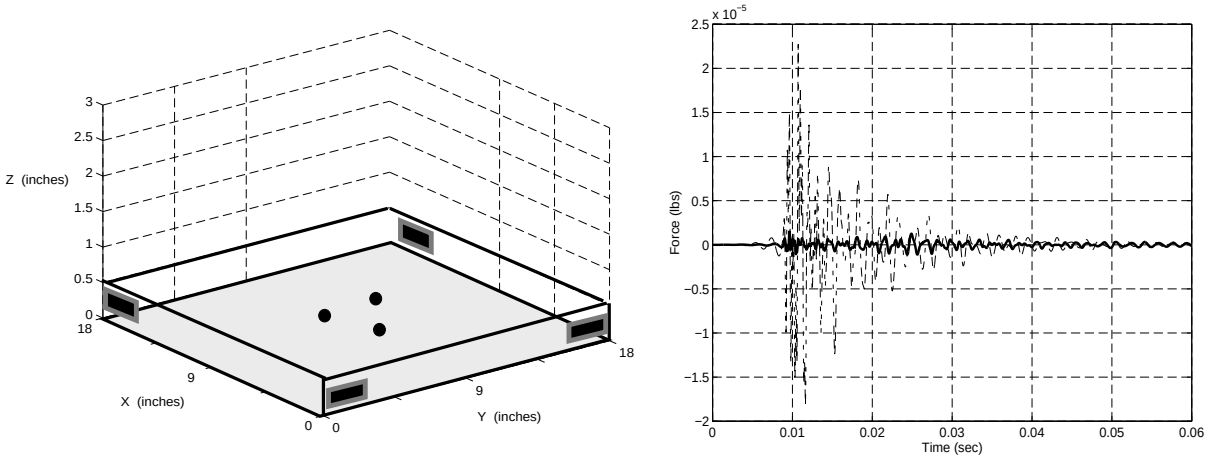

Figure 5: *Locations of the actuators and sensors chosen by the broadband QR method (left). The uncontrolled (dashed) and the controlled (solid) time-domain impulse responses for the control bandwidth for the connector located at* $x = 17in.$, $y = 17in.$ *(right).*

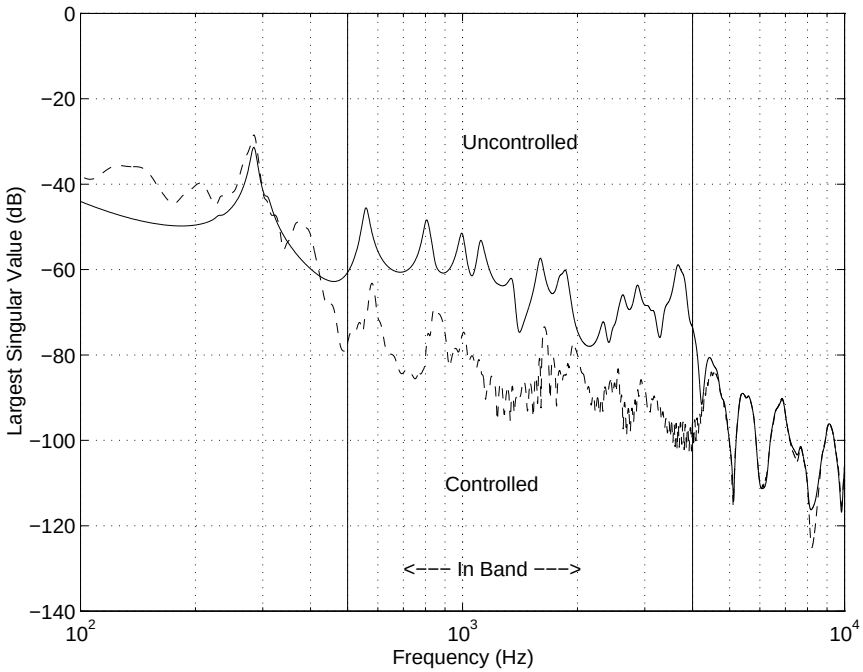

Figure 6: *Plot of the largest singular values of the uncontrolled (solid) and the controlled (dashed) responses at all four feet for the configuration chosen by the QR algorithm.*

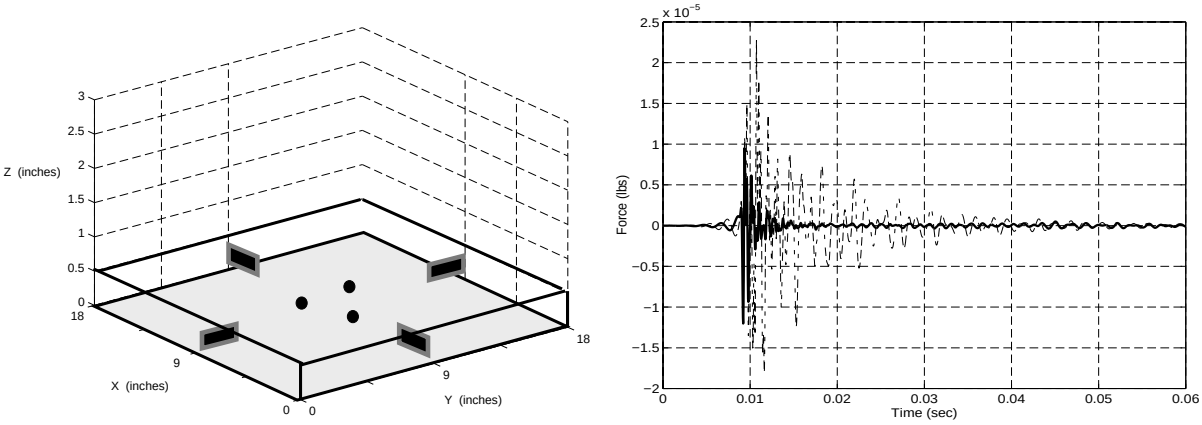

Figure 7: *Locations of the actuators and sensors chosen by the authors for comparison to the QR method (left). The uncontrolled (dashed) and the controlled (solid) time-domain impulse responses for the control bandwidth for the connector located at* $x = 17in.$, $y = 17in.$ *(right).*

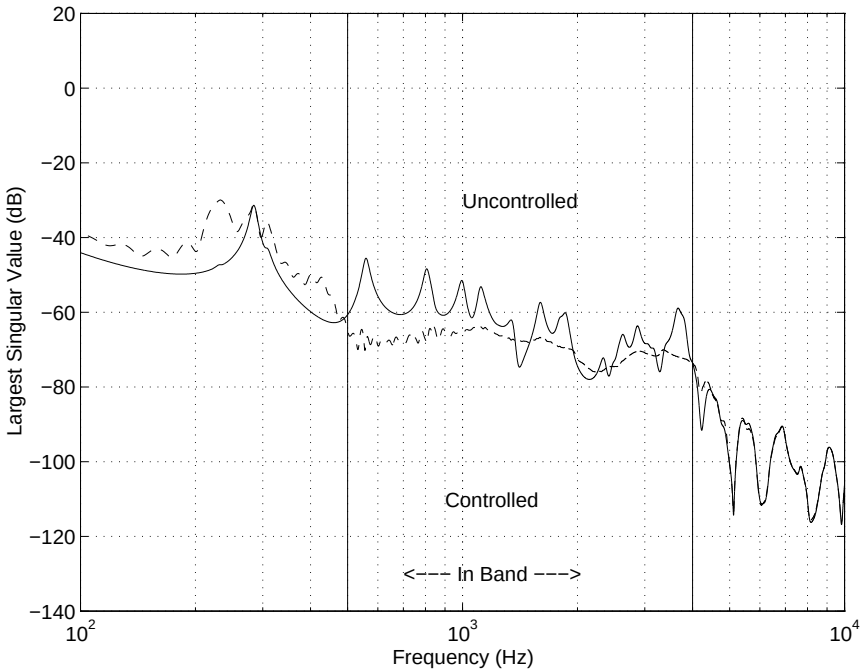

Figure 8: *Plot of the largest singular values of the uncontrolled (solid) and the controlled (dashed) responses at all four feet for the configuration chosen by the authors.*

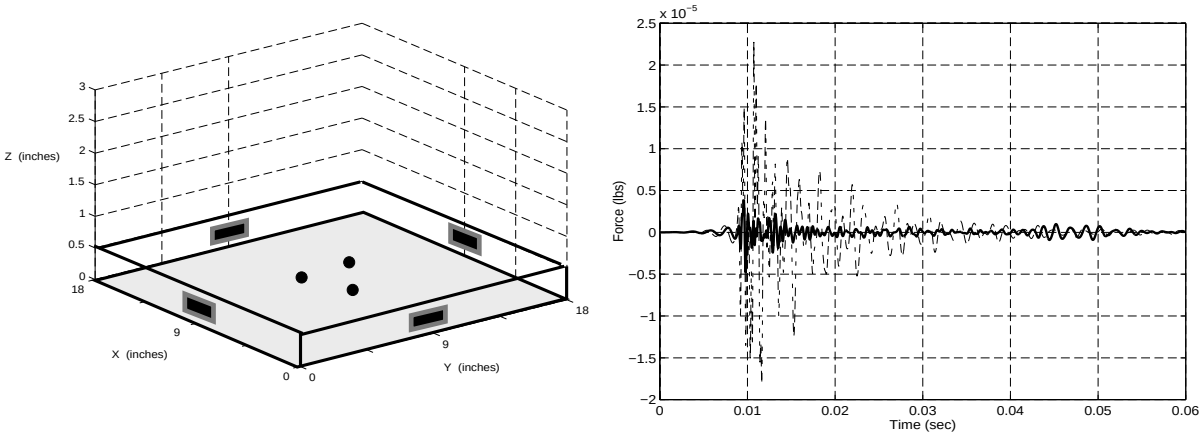

Figure 9: *Locations of the actuators and sensors chosen by the authors for comparison to the QR method (left). The uncontrolled (dashed) and the controlled (solid) time-domain impulse responses for the control bandwidth for the connector located at* $x = 17in.$, $y = 17in.$ *(right).*

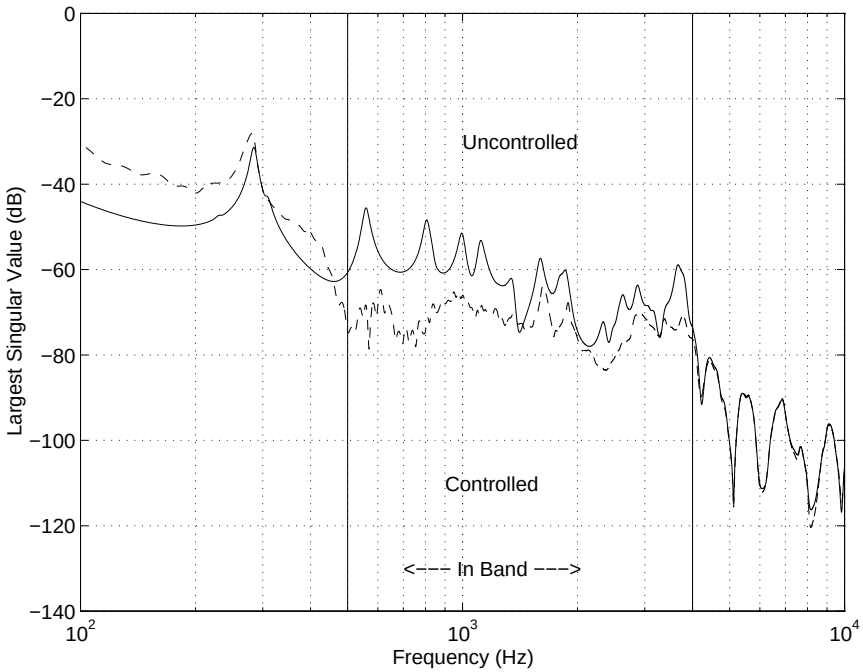

Figure 10: *Plot of the largest singular values of the uncontrolled (solid) and the controlled (dashed) responses at all four feet for the configuration chosen by the authors.*